New archeointensity data from Novgorod (North-Western Russia) between c. 1100 and 1700 AD. Implications for the European intensity secular variation

Natalia Salnaia, Yves Gallet, Agnès Genevey, Ilya Antipov

New archeointensity data from Novgorod (North-Western Russia) between c. 1100 and 1700 AD. Implications for the European intensity secular variation

Natalia Salnaia[1], Yves Gallet[2], Agnès Genevey[3], Ilya Antipov[4]

[1] Institute of Physics of the Earth, Russian Academy of Sciences, Moscow, Russia, natasavi@inbox.ru, corresponding author

[2] Institut de Physique du Globe de Paris- Sorbonne Paris Cité- Université Paris Diderot, UMR 7154 CNRS, Paris, France

[3] Sorbonne Universités, UPMC Univ. Paris 6, CNRS, UMR 8220, Laboratoire d'archéologie moléculaire et structurale (LAMS), Paris, France

[4] Institute of History, St Petersburg State University, St Petersburg, Russia

Abstract

Reconstructing the secular variation of Europe's geomagnetic field over the past millennium is challenging because of the lack of recently acquired archeomagnetic data from Western Russia. In this paper, we report on nine new archeointensity values obtained from groups of brick fragments sampled in Novgorod (North-Western Russia) and its vicinities. These fragments were collected from churches whose precise ages range from the beginning of the 12th century to the end of the 17th century AD. All the archeointensity measurements were carried out using the Triaxe experimental protocol, which takes into account the thermoremanent magnetization (TRM) anisotropy effect. Intensity determinations were performed using fast and slow cooling rates for laboratory-TRM acquisition. The results confirm that the Triaxe protocol overcomes the TRM cooling rate dependence. The new data shows that geomagnetic field intensities in North-Western Russia have decreased in the past millennium. Comparisons were made with other data previously obtained in Western Europe,

the Balkans and Russia, as well as with intensity values expected in Novgorod from global geomagnetic field models. These comparisons yielded three main results: 1) The new archeointensity data do not show the occurrence of large intensity variations in North-Western Russia, as those observed in the Balkan dataset. Conversely, they appear more compatible with Western European results, which suggests a limited non-dipole field effect across Europe during the past millennium; 2) Our data are weaker than the intensity values expected in Novgorod from the available global geomagnetic field models. This suggests that the field models are inaccurate for the Novgorod area; 3) A constant linear decrease of the geocentric axial dipole moment since 1600 AD does not appear compatible with our younger data.

Keywords: Secular variation, geomagnetic field intensity, past millennium, North-Western Russia, Europe, geomagnetic field modeling.

1. Introduction

For the past 15 years, considerable efforts have been made to improve our knowledge of the secular variation in Western Eurasia's geomagnetic field over the past few millennia. In Western Europe, these efforts were focused on the recovery of both the directional (e.g. Gallet et al., 2002; Hervé et al., 2013a) and field intensity variations for the period spanning the past two to three millennia, with significant progress (e.g. Gómez-Paccard et al., 2008; 2012; 2016; Gallet et al., 2009; Genevey et al., 2009; 2013; 2016; Hervé et al., 2013b; 2016).

The overall geomagnetic field intensity variation curve in Western Europe, which covers the past three millennia, is now one of the best documented and detailed curve worldwide. However, certain segments remain poorly constrained, suffering from an insufficient number of data as is, for instance, the case for the first millennium BC (Hervé et al., 2013b; 2016). In contrast, the past 1500 years are particularly well documented, revealing a geomagnetic signal punctuated by a series of centennial-scale intensity peaks (Genevey et al., 2013; 2016). This well-defined curve demonstrates that recovering the intensity secular variation at the centennial time scale is a difficult but achievable target.

At present, only the important dataset obtained in the Balkans (South-Eastern Europe) including results from Bulgaria (Kovacheva et al., 2014), Greece (e.g. Tema and Kondopoulou, 2011; Tema et al., 2012) and Southern Italy (e.g. Tema et al., 2013) can be used to carry out a comparison between the geomagnetic intensity variations that occurred in Western and Eastern Europe (e.g. Genevey et al., 2013, 2016; Pavón-Carrasco et al., 2014a). The Balkan data appear rather dispersed. They exhibit large intensity fluctuations with trends like those observed in Western Europe, though with higher amplitude. The resolution of this curve, however, does not have enough detail to conclude on the occurrence of drifting non-dipole sources, westward nor eastward, between Western and Eastern Europe during the past 1500 years (Genevey et al., 2016). Given the available data, Pavón-Carrasco et al. (2014a) concluded that the geomagnetic field intensity evolution over the past few millennia was likely homogeneous across Europe.

In other sub-regions of Europe, archeointensity data are still not numerous enough to further constrain the issue of homogeneity in intensity variations over this semi-continental wide area. This is the case for North-Western Russia, around the city of Novgorod (λ=58.52°N, ϕ=31.27°E). Here archeointensity data dated to the Medieval period and meeting minimum quality criteria are virtually absent (e.g. Burlatskaya et al., 1986; Genevey et al., 2008; Pavón-Carrasco et al., 2014a). During the first half of the second millennium AD, this region was economically rich because of active trading with other Russian lands and the Baltic Sea countries (Rybina, 1992; 2001). Many buildings, especially churches were built at that time using baked-clay bricks, which makes this region a promising target for an archeomagnetic study. New archeointensity results from this region could further be used to test (and later to improve) the reliability of the available global archeomagnetic field models (e.g. Licht et al., 2013; Pavón-Carrasco et al., 2014b; Nilsson et al., 2014.). In this paper, we report on new archeointensity data obtained from the Novgorod area, dated between c. 1100 AD and c. 1700 AD.

2. Archeomagnetic sampling

All archeological fragments analyzed in this study consist of baked clay bricks collected from churches located in Novgorod (North-Western Russia) and its surroundings (Fig. 1). The oldest reference to the city of Novgorod goes back to the middle of the 9th century AD, making it one the most ancient Russian cities. During the 10th century AD, Novgorod was already a prosperous city because of its position on the trading route from the Varangians (i.e. the other name of Vikings) to the Greeks. Between the 11th and the 15th centuries, Novgorod was the capital city of the Novgorodian Republic, which extended from the Baltic to Northern Urals. This republic ended in 1478 AD when its territory became annexed to the state of Muscovy under the reign of Ivan III. During the republic period, many churches were built in the city of Novgorod and in nearby monasteries using bricks, local stones, or a combination of both. The construction date of these churches is known within a 1-7-yr uncertainty thanks to historical sources such as the Novgorod first chronicle (Fig. 2, Table 1; Nasonov, 1950; English translation in Michell and Forbes, 1914).

It is important to emphasize that the bricks used for construction are of local origin. The craftsmen benefited from abundant clay sources near Novgorod, which allowed the development of important pottery production activity, likely accompanied by brick manufacturing (e.g. Antipov and Gervais, 2015). The local origin of the bricks is also verified through the discovery of a kiln at Ryurik Gorodishche, an area approximately 2 km south of the Novgorod center (Gervais and Lipatov 2003; Lipatov, 2005), whose brick production activity served to build the church of the Annunciation in the Gorodishche (site BGA01; Fig. 2a, Table 1) in 1103 AD. Recently, the continuous activity of brick production in Novgorod with a regional distribution was further substantiated by the discovery of a ship carrying a load of bricks that sunk to the bottom of the Volkhov river (Antipov and Gervais, 2015). Interestingly, no evidence for an active brick market in Novgorod during the Middle Ages was found in the archives, nor for a large storage space for the fabricated bricks within the city. This indicates that the time delay between the production and the use of the bricks was most probably very short and the bricks were likely fired on request for specific buildings.

The archeomagnetic sampling of bricks was performed either on still standing churches or on vestiges found during excavations (Fig. 3). We note that the typology evolution of the bricks (see description and discussion in Antipov and Gervais, 2015) provided us with an additional guide for only selecting the bricks used in the original phase of the buildings, thus avoiding the bricks used in possible late renovations, or for identifying the bricks from different construction phases. Here we present new archeointensity data obtained from nine groups of brick fragments sampled from the remains of different churches. The bricks were dated from the beginning of the 12th century to the end of the 17th century AD (Table 1). The age distribution is inhomogeneous: four groups for the 12th and three for the 14th centuries. The absence of fragments from the 13th century is linked to the Mongol invasion of 1238-1240 AD. Although the invasion did not destroy the city of Novgorod, it caused a marked slowdown in regional economic activity and thus led to a limited number of new constructions during most of this century.

3. Acquisition of new archeointensity data

3.1. Methods

Archeointensity data were obtained using the experimental protocol developed for the Triaxe magnetometer (Le Goff and Gallet, 2004). The Triaxe is a vibrating sample magnetometer that allows continuous high-temperature (up to 670°C) magnetization measurements of a small (<1 cm^3) cylindrical sample. It further allows the acquisition of a thermoremanent magnetization (TRM) in any direction and in a field intensity up to 200 μT. Le Goff and Gallet (2004) designed an automated routine for intensity determinations that involves a succession of five series of measurements performed between two temperatures referred to as T1 and T2. T1 is generally set to 150°C and T2, in the present study, was chosen between 440°C and 520°C depending on the specimens (see below). The NRM of the specimen is first demagnetized up to T2 (first series of measurements), while the thermal variations between T1 and T2 of the magnetization fraction still blocked above T2 are recorded twice during the second (between T2 and T1) and third series of measurements (between T1 and T2). A laboratory TRM is then acquired between T2 and T1 (fourth series of measurements), which is demagnetized up to T2 during the fifth series of measurements. The protocol ends with the cooling of the specimen down to room temperature. Intensity determinations are derived from the magnetization data acquired every 5°C during the first, third and fifth series of measurements, i.e. in the very same heating conditions between T1 and T2. These measurements can be expressed through two ratios, which are multiplied by the field intensity used for laboratory-TRM acquisition, and defined as R(Ti) and R'(Ti) in Le Goff and Gallet (2004). R(Ti) is the ratio between the NRM and TRM fractions with unblocking temperatures between the running temperature Ti and T2, whereas R'(Ti) is the ratio between the NRM and TRM fractions unblocked between T1 and Ti. Le Goff and Gallet (2004) experimentally showed that R(Ti) is more prone to cooling rate effect over TRM acquisition at higher temperatures than R'(Ti). For this reason, the mean intensity values are derived at the specimen level from R'(Ti) data.

A great asset of the Triaxe protocol is that it avoids a correction for the TRM anisotropy effect because the laboratory TRM is acquired so that its direction is parallel to that of the NRM. A description of the procedure is provided in Le Goff and Gallet (2004) (see also in Genevey et al., 2008 for a general discussion on the TRM anisotropy effect). Thanks to numerous comparative tests with data obtained using more classical intensity techniques (Thellier-Aitken/-Coe/-IZZI methods; Thellier and Thellier, 1959; Aitken et al., 1988; Coe, 1967; Yu et al., 2004) implying magnetization measurements at ambient temperature, it was also experimentally observed that the R'(Ti) intensity determinations account for the cooling rate effect on TRM acquisition (Le Goff and Gallet, 2004; Gallet and Le Goff, 2006; Genevey et al., 2009; Hartmann et al., 2010; 2011 and see in Section 3c below). Furthermore, any bias in the intensity data possibly induced by the presence of multi-domain grains in the specimen is mitigated because the laboratory TRM is acquired under similar conditions as those of the NRM.

In the present study, the reliability of the Triaxe data relies on the same set of selection criteria used by Genevey et al. (2013; 2016) and Hartmann et al. (2010; 2011). These criteria aim to insure the nominal paleomagnetic behavior described in Le Goff and Gallet (2004), which is characterized, in particular, by a "primary" univectorial magnetization component isolated between T1 and T2, with the possibility to adjust a posteriori T1 to a higher temperature (referred to T1') in case of a secondary magnetization component, and by rather constant R'(Ti) data over this temperature range (i.e. with an overall slope "S" of less than 10%). Rock magnetic analyses, including low-field magnetic susceptibility vs temperature, isothermal remanent magnetization (IRM) acquisition, hysteresis measurements, and three-axis IRM demagnetization were also carried out on the fragments. These additional analyses constrain the nature and stability upon heating of their magnetic mineralogy.

3.2. Magnetic mineralogy

As a preliminary test for selecting the most promising fragments for intensity experiments, low-field magnetic susceptibility vs temperature curves were systematically acquired up to ~530-550°C on the whole collection using a Kappabridge MFK1 coupled with a CS4 thermal unit (Agico, Czech Republic). The first objective of these measurements was to test the thermal stability of the magnetic mineralogy inferred from the reversibility between the heating and cooling curves over the typical temperature range of intensity determinations. This is the reason why the thermomagnetic analyses were essentially performed up to a temperature relatively close to T2. Every fragment that was retained displays reversible behavior in susceptibility, as in Fig. 4a-e, whereas Fig. 4f illustrates a rejected fragment. We note that only two fragments were rejected at this step, which indicates magnetic stability upon heating of our collection of bricks. For a few fragments successfully analyzed in intensity, additional thermomagnetic measurements were also conducted at higher temperatures on new fresh powders, up to 700°C (insets in Fig. 4). They show a clear inflexion point between ~520°C and the Curie temperature of magnetite. The presence of hematite is also implied in several fragments (e.g. Fig. 4b).

In order to decipher the nature of the magnetic carriers in the fragments that met our archeointensity selection criteria, IRM and hysteresis measurements were performed on all the retained fragments. They were carried out up to 0.9 T using a Variable Field Translation Balance (VFTB; Peterson Instruments, Germany). IRM curves show that the magnetization is never saturated at 0.9 T, which indicates the presence of minerals with high-coercivity, such as hematite (Fig. 5a). We observe, however, a high variability in the IRM behavior. This indicates variable proportions of this high-coercivity fraction against one characterized by lower coercivity. Some fragments (for instance PP01-05; PP01-12; BGA01-02; Fig. 5a) clearly exhibit around 0.1-0.2 T a plateau or a sharp inflection in the saturation curves. This likely emphasizes the joint presence of minerals from the (titano)magnetite family. In all cases, the hysteresis loops are constricted (Fig. 5b-d): this confirms that the magnetic mineralogy of our fragments consists of minerals with different coercivities.

For fragments fulfilling our archeointensity selection criteria (except six of them for which not enough material was remaining), we completed the previous measurements with thermal demagnetization of a three-axis IRM (1.2T, 0.4T, 0.2T) imparted in perpendicular directions (Lowrie, 1990). Three main categories of behavior are distinguished. In the first category (Fig. 5e), the low-coercivity fraction, most likely consisting of (titano)magnetite, largely dominates any other component of the magnetic mineralogy. The thermal demagnetization of this fraction is achieved around 550°C. This category represents about 20% of the collection of fragments. In the second category (Fig. 5f), which is most frequent in our collection (about 50%), there is a higher proportion of high-coercivity minerals that is demagnetized around 200°C. This fraction is sometimes as large as that of low coercivity. In this case, the low-coercivity fraction predominates the magnetic signal between ~200°C and 500/550°C. Although the presence of goethite cannot be excluded in our fragments on the basis of these experiments, it seems more probable that we observe the mineral of high coercivity and low unblocking temperature (HCLT), which is commonly present in archeological baked clays (e.g. McIntosh et al., 2011; Hartmann et al., 2011; Genevey et al., 2016). Lastly, the third category (about 30% of the collection) is characterized by a high-coercivity fraction, which remains present, and in a few cases, predominates the magnetization throughout the thermal demagnetization sometimes achieved above 600°C (Fig. 5g). Over a wide temperature range, the magnetization is thus carried both by low-coercivity and high-coercivity minerals, which are most likely composed of (titano)magnetite and hematite.

As a synthesis, the rock magnetic analyses indicate that the magnetic mineralogy of our fragments includes three types of minerals with different coercivities and different unblocking temperatures in various proportions. These are likely (titano)magnetite, hematite, and the HCLT mineral. The latter can be a substituted form of hematite. It is worth mentioning that a similar combination of magnetic carriers is commonly found in archeomagnetic studies (e.g. Genevey et al., 2016).

Finally, we performed a series of specific archeointensity experiments on fragments belonging to the third IRM category described above. The aim was to ensure that, despite a significant proportion of hematite, these fragments provide a reliable value of the ancient geomagnetic field intensity. For these fragments, which are characterized by a magnetic mineralogy stable upon heating, a total pseudo-NRM was first acquired in a known laboratory field condition. In a second step, classical Triaxe archeointensity measurements were performed to analyze this pseudo-NRM. The latter allow to recover very precisely, to within a few %, the value of the field intensity used for the pseudo-NRM acquisition (Fig. S1 in supplementary material). These measurements therefore demonstrate that the hematite-related magnetization component does not significantly disturb the determination of the ancient field intensity that it is likely conveyed by the magnetization carried by (titano)magnetite.

3.3. Cooling rate effect on TRM acquisition

In several specimens, a rather specific behavior of the R(Ti) and R'(Ti) data was observed, that is characterized first, by a significant increase of the R(Ti) data with the temperatures and second, by a pronounced concave evolution of the R'(Ti) data (see two examples in Fig. 6a,c). In several cases, the strong concavity of the R'(Ti) curves implied the rejection of the corresponding specimens.

Per the experiments performed by Le Goff et Gallet (2004), the significant increase in R(Ti) data led us to suspect a strong cooling rate effect on TRM acquisition (see Section 5 and Fig. 4 in Le Goff and Gallet, 2004, and in Genevey et al., 2008 for a more general discussion on the cooling effect on TRM acquisition). It is worth recalling that Le Goff and Gallet (2004) experimentally observed that the increasing trend in R(Ti) data can be linked to the fact that the cooling rate effect becomes stronger as the magnetization fractions with unblocking temperatures between Ti and T2 gradually decrease. Le Goff and Gallet (2004) further showed that this difficulty can be circumvent by considering R'(Ti) data relying on the magnetization fractions unblocked between T1 and Ti. In the present study, however, it was important to confirm this characteristic because the cooling rate effect appeared potentially strong. For this reason, we analyzed many fragments using (for different specimens) two cooling rates for the laboratory-TRM acquisition: 1- the one used for routine measurements carried out using the Triaxe, i.e. with a cooling rate fixed to 25°C/minute and 2- a cooling rate reduced to 2°C/minute (see details in Table S1 in supplementary material). In the latter case, the R'(Ti) data often exhibit a more suitable behavior with more constant values, while the R(Ti) data show less increase over the temperature interval of analysis (Fig. 6b,d).

We then directly compared the intensity values computed at the group level (Fig. 7) using either the 25°C/minute cooling rate or the 2°C/minute cooling rate. This comparison shows no statistical significance in the difference, which remains within 5% when the intensity determinations obey our selection criteria. Moreover, on average (31 fragments) the differences in intensity at the fragment level relative to the values obtained using a cooling rate of 25°C/minute are also insignificant: 1.5±2.8%. Nevertheless, the use of a slow cooling rate of 2°C/minute allowed us to retain several fragments that would have been rejected otherwise. This led us to retain the group of fragments GYU01, for which one fragment among the three was only successfully analyzed using the slow cooling rate (GYU01-04; Table S1 in supplementary material). Hereafter, we will therefore determine mean intensity values at the fragment level by combining the values obtained whatever the cooling rate applied. Finally we note that for some specimens, T2 was chosen relatively low (440°C; Table S1 in supplementary material), assuming that the cooling rate dependence on TRM acquisition was more pronounced for the magnetization fraction unblocked at high temperatures (Le Goff and Gallet, 2004).

3.4. Archeointensity data

Our experiments allowed us to obtain archeointensity data satisfying our selection criteria from 165 specimens (of a total of 337 specimens whose magnetization was strong enough for the Triaxe magnetometer). These specimens are from 40 different fragments, with usually 3 to 4 specimens successfully analyzed per fragment (see Table 1 in Supplementary material). This corresponds to a rate of success comprised between 42% and 67% depending on the groups of fragments (Table S1 in supplementary material). Failures were linked, in equal proportion, to a strong concavity of the R'(Ti) curve (Fig. 6c), a large slope of the R'(Ti) curve or to a difference between specimen values from a same fragment larger than our 5% limit. Typical examples of thermal demagnetization data for successful specimens are reported in Fig. S2 (in supplementary material). Mean intensity values were derived for nine groups of fragments, with a minimum number of three fragments per group (VS01, GYU01). This number increases up to five for four groups (DM03, DM02, BGA01, SH01) and six for group PP01. Fig. 8 illustrates the archeointensity data obtained from six different groups of fragments (one panel per group). In this representation, each curve exhibits the R'(Ti) data obtained for one specimen. The curves also represent the scatter in the data obtained from each group. Here, we observe that the variability is quite weak, which was expected given the excellent temporal homogeneity of the fragments from each group.

As in all the previous studies dealing with Triaxe intensity data (e.g. Genevey et al, 2013; Gallet et al, 2014), we estimated a mean archeointensity value for each group of fragments via first the averaging of the R'(Ti) data obtained for each specimen, then the averaging of these specimen values at the level of each fragment, and finally the averaging of the fragment values at the group level. The group-mean archeointensity results are well defined, with standard deviations consistently less than 2.6 μT and not exceeding 5% of the corresponding group-mean value (between 1.2% and 4.2%). They range from 66.1±1.9 μT to 48.7±1.6 μT, with an overall decrease of the geomagnetic field intensities between the 12th and 17th centuries AD (Table 1; Fig. 9).

4. Discussion

Fig. 9a shows the data available within a radius of 700 km around Novgorod (grey dots). Apart from the new archeointensity results reported in the present study, the previous data were principally obtained from two areas (Fig. 1a) around Moscow and Vologda (~500 km from Novgorod). Although the data were obtained over 30-years-ago (Burlatskaya et al., 1986), partial-TRM checks were used most often to test the stability of the magnetic mineralogy on heating (Genevey et al., 2008). Here we only retained the data with partial-TRM checks and those for which the standard deviation is less than 15% of the corresponding mean intensity value. Note that the corresponding fragments were collected from architectural bricks, a material for which the TRM anisotropy effect is expected to be weak (e.g. Genevey et al., 2008). A color code in Fig. 9a allows one to distinguish between results obtained from two or more independent archeological artifacts. Two main remarks can be made about these data. Firstly, within the ~1500-1800 AD time interval, they are very scattered regardless of the number of fragments or specimens used to estimate the mean intensity values, which prevents a clear determination of the geomagnetic field intensity evolution. Such a scatter clearly casts doubt on the reliability of at least some of these data. Secondly, no result was available up to now from North-Western Russia for the ~1000-1400 AD time interval.

While our new data exhibits an overall decreasing trend in geomagnetic field intensity over the time interval of concern, they do not show a variability that could indicate the occurrence of rapid and large-amplitude intensity fluctuations in North-Western Russia during the past millennium. In this respect, although it is acknowledged that the present dataset contains only nine archeointensity values, they do not corroborate the large variations observed in the Balkan region (700 km around Thessaloniki; Tema and Kondopoulou, 2011; Kovacheva et al., 2014). This difference is illustrated in Fig. 9a, where the Balkan data (light violet squares) are reported after their transfer to the latitude of Novgorod using the Virtual Axial Dipole Moment approximation. Here we recognize that this approach adds uncertainties on the transferred values (e.g. Casas and Incoronato, 2007); however we assume that they remain relatively limited compared to the experimental and age uncertainties of the data. For the latter dataset, a color code is used to distinguish between results with and without partial-TRM checks (see discussion in Genevey et al., 2013; 2016). This distinction does not, however, allow one to detect any difference in the nature of the intensity fluctuations in the Balkans. In contrast, the Novgorod results appear in better agreement with the average geomagnetic field intensity variation curve for Western Europe (700 km around Paris; blue curve in Fig. 9a), also transferred to the latitude of Novgorod, determined by Genevey et al. (2013; 2016). However, the available data are still not numerous enough to show the occurrence of similar short-lasting relative maxima in North-Western Russia as those observed in Western Europe, i.e. dated from the 12th century, the second half of the 14th century and around 1600 AD (Genevey et al., 2016). At present, the archeointensity dataset from the Novgorod area is more compatible with homogeneous geomagnetic field intensity variations throughout Europe over the past millennium (e.g. Pavón-Carrasco et al., 2014a).

In Fig. 9b, the new archeointensity data are also compared with the expected intensity values computed at Novgorod from recent global archeomagnetic field models (i.e. A_FM, Licht et al., 2013; SCHA_DIF.14k, Pavón-Carrasco et al., 2014b; pfm9k.1a, Nilsson et al., 2014). Note that the curve derived from pfm9k.1a (brown curve) displays smoother variations than those from the two other models (green curve, A_FM; orange curve, SCHA-DIF.14k), which is due to the use of sedimentary, volcanic and archeological data by Nilsson et al. (2014) (for instance, see discussion in Licht et al., 2013). Nevertheless, in all three cases, the models quasi-systematically predict intensity values that are statistically higher than the data obtained in the Novgorod area. This indicates that the global field models need to be revised to correct for this intensity over-estimation in North-Western Russia. It is possible that at least a part of this offset originates from the cooling rate effect, which was considered only for a small proportion of the archeointensity data used for field modeling (Genevey et al., 2008; Brown et al., 2015).

The most recent archeointensity result obtained in Novgorod, i.e. from group DM03 precisely dated to the end of the 17th century (Table 1), is also of special interest for field modeling. Its value is lower by ~5 μT than the expected intensity around the same epoch which was derived from the historical geomagnetic field modeling referred to as gufm1 (black curve in Fig. 9b; Jackson et al., 2000). Briefly, it is worth recalling that the latter field models were built using magnetic field measurements made by mariners and performed in a few land observatories (e.g., Jonkers et al., 2003), and assuming a linearly decreasing geocentric axial dipole field moment (term g_1^0) from ~1600 AD to the present (Barraclough, 1974). Such hypothesis made for the 1600-1840-time interval (i.e. beyond the first direct intensity measurements) is not confirmed here. Even though differences appear less pronounced, our value also fails to confirm a constant -or nearly constant g_1^0 evolution between ~1600 and 1840, as previously proposed by Finlay (2008) and Gubbins et al. (2006), respectively (Fig. 9b). On the other hand, its age cannot help deciphering the oscillatory g_1^0 evolution suggested by Genevey et al. (2009) over the past four centuries (see also Hartmann et al., 2011 for Brazilian data). More archeomagnetic data are clearly needed to strengthen this important issue.

5. Conclusions

This study is part of a project, which aims to acquire archeomagnetic data acquisition from Central and North-Western Russia. Previous studies were consistently made during the 70s and 80s, but unfortunately stopped for many years. At the same time, other Western Eurasian regions benefited from a strong development in archeomagnetism research activity.

We investigated several groups of architectural brick fragments collected from old churches in the Novgorod area. These groups are precisely dated between the 12th and 17th century AD.

Archeointensity analyses were carried out using the experimental protocol developed for the Triaxe magnetometer. They allow us to obtain nine new mean archeointensity data, derived from 40 different fragments and 165 analyzed specimens.

These data show an overall decreasing trend in geomagnetic field intensity over the past millennium, with no evidence of rapid variations with large amplitude such as those proposed from the Balkans (e.g. Tema and Kondopoulou, 2011; Kovacheva et al., 2014). They are more compatible with the French geomagnetic field intensity variation curve proposed by Genevey et al. (2016), after its transfer to the latitude of Novgorod. Should this result persist in future archeointensity data collections and analyses, the intensity secular variation would have remained homogeneous across all Europe during at least the past millennium.

An intriguing observation is that our Novgorod results are lower than the intensity values predicted from archeomagnetic field models. We suggest that the observed differences, at least in part, originate from the cooling rate effect on TRM acquisition, the latter not considered in most of the data used for the construction of the models.

Finally, we note that a result dated to the end of the 17th century is not compatible with the expected intensity value derived from the gufm1 model (Jackson et al., 2000), which assumes a linear decrease of the axial dipole moment over the past four centuries.

Acknowledgments

This study was financed by grant N 14.Z50.31.0017 of the Russian Ministry of Science and Education. We are very grateful to Maxime Le Goff for his unwavering technical assistance. We thank two anonymous reviewers for their helpful comments. This is IPGP contribution no. 3842.

References

Aitken, M. J., Allsop, A. L., Bussell, G. D., Winter, M. B., 1988. Determination of the intensity of the Earth's magnetic field during archaeological times: Reliability of the Thellier technique. Rev. Geophys. 26, 3-12.

Aitken, M. J., Allsop, A. L., Bussell, G. D., Liritzis, Y., Winter, M. B., 1989. Geomagnetic intensity measurements using bricks from Greek churches of the first and second millennia A.D.. Archaeometry 31, 77–87.

Antipov, I., Gervais, A., 2015. The bricks from St Nicholas church at Lipno near Novgorod (1292) and the origins of the new Novgorodian building tradition. Estonian Journal of Archaeology 19, 58-7.

Barraclough, D., 1974. Spherical harmonic analysis of the geomagnetic field for eight epochs between 1600 and 1910. Geophys. J. R. Astron. Soc. 43, 497–513.

Brown, M. C., Donadini, F., Korte, M., Nilsson, Korhonen, K., Lodge, A., Lengyel, S. N., Constable, C. G., 2015. GEOMAGIA50.v3: 1. General structure and modifications to the archeological and volcanic database. Earth Planet and Space 67, 1-31.

Burlatskaya, S. P., Nachasova, I.E., Didenko, E. J., Shelestun, N. K., 1986. Archeomagnetic determinations of geomagnetic field elements. Sov. Geophys. Comm. of the USRR Acad. of Sci., Moscow.

Casas, L., Incoronato, A., 2007. Distribution analysis of errors due to relocation of geomagnetic data using the ‘Conversion via Pole’ (CVP) method: implications on archeomagnetic data. Geophys. J. Int. 169, 448–454.

Coe, R. S., 1967. Paleo-Intensities of the Earth's magnetic field determined from Tertiary and Quaternary Rocks. J. Geophys. Res. 72, 3247–3262.

De Marco, E., Spatharas, V., Gómez-Paccard, M., Chauvin, A., Kondopoulou, D., 2008. New archaeointensity results from archaeological sites and variation of the geomagnetic field intensity for the last 7 millennia in Greece. Phys. Chem. Earth 33, 578–595.

Finlay, C.C., 2008. Historical variation of the geomagnetic axial dipole. Phys. Earth Planet. Inter. 170, 1-14.

Gallet, Y., Genevey, A., Le Goff, L., 2002. Three millennia of directional variation of the Earth’s magnetic field in western Europe as revealed by archeological artefacts. Phys. Earth Planet. Inter. 131, 81-89.

Gallet, Y., Le Goff, M., 2006. High-temperature archeointensity measurements from Mesopotamia. Earth Planet. Sci. Lett. 241, 159-173.

Gallet, Y., Genevey, A., Le Goff, M., Warmé, N., Gran-Aymerich, J., Lefèvre, A., 2009. On the use of archeology in geomagnetism, and vice-versa: Recent developments in archeomagnetism. C. R. Physique, 10 630–648.

Gallet, Y., D'Andrea, M., Genevey, A., Pinnock, F., Le Goff, M., Matthiae, P., 2014. Archaeomagnetism at Ebla (Tell Mardikh, Syria). New data on geomagnetic field intensity variations in the Near East during the Bronze Age. J. Archaeol. Sci. 42, 295-304.

Genevey, A., Gallet, Y., Constable, C., Korte, M., Hulot, G., 2008. ArcheoInt: An upgraded compilation of geomagnetic field intensity data for the past ten millennia and its application to the recovery of the past dipole moment. Geochem. Geophys. Geosys. 9(4), Q04038.

Genevey, A., Gallet, Y., Rosen, J., Le Goff, M., 2009. Evidence for rapid geomagnetic field intensity variations in Western Europe over the past 800 years from new archeointensity French data. Earth Planet. Sci. Lett. 284, 132-143.

Genevey, A., Gallet, Y., Thébault, E., Jesset, S., Le Goff, M., 2013. Geomagnetic field intensity variations in Western Europe over the past 1100 years. Geochem. Geophys. Geosyst. 14/8, 2858-2872.

Genevey, A., Gallet, Y., Jesset, S., Thébault, E., Bouillon, J., Lefèvre, A., Le Goff, M., 2016. New archeointensity data from French Early Medieval ceramic production (6th-10th century AD). Tracing 1500 years of geomagnetic field intensity variations in Western Europe. Phys. Earth Planet. Inter. 257, 205-219.

Gervais, A. V., Lipatov A. A., 2003. The interpretation problems of the kiln near the Annunciation church on Gorodishche (in Russian). In Novgorod i Novgorodskaia zemlia. Istoria i archeologia. V. Novgorod 17, 344–350.

Gómez-Paccard, M., Chauvin, A., Lanos, P., Thiriot, J., 2008. New archeointensity data from Spain and the geomagnetic dipole moment in western Europe over the past 2000 years. J. Geophys. Res., 113, B09103.

Gómez-Paccard, M., Chauvin, A., Lanos, P., Dufresne, P., Kovacheva, M., Hill, M. J., Beamud, E., Blain, S., Bouvier, A., Guibert, P., and Archaeological Working Team, 2012. Improving our knowledge of rapid geomagnetic field intensity changes observed in Europe between 200 and 1400 AD. Earth Planet. Sci. Lett. 355–356, 131–143.

Gómez-Paccard, M., Osete, M.L., Chauvin, A., Pavón-Carrasco F.J., Pérez-Asensio, M., Jiménez, P., Lanos, P, 2016. New constraints on the most significant paleointensity change in Western Europe over the last two millennia. A non-dipolar origin?. Earth Planet. Sci. Lett. 454, 55-64.

Gubbins, D., Jones, A.L., Finlay, C.C., 2006. Fall in Earth's magnetic field is erratic. Science 312, 900-902.

Hartmann, G., Genevey, A., Gallet, Y., Trindade, R., Etchevarne, C., Le Goff, M., Afonso, M., 2010. Archeointensity in Northeast Brazil over the past five centuries. Earth Planet. Sci. Lett. 296, 340-352.

Hartmann, G., Genevey, A., Gallet, Y., Trindade, R., Le Goff, M., Najjar, R., Etchevarne, C., Afonso, M., 2011. New historical archeointensity data from Brazil : Evidence for a large regional non-dipole field contribution over the past few centuries. Earth Planet. Sci. Lett. 306, 66-76.

Hervé, G., Chauvin, A. Lanos P., 2013a. Geomagnetic field variations in Western Europe from 1500 BC to 200 AD. Part I: Directional secular variation curve. Phys. Earth Planet. Inter. 218, 1-13.

Hervé, G., Chauvin, A. Lanos P., 2013b. Geomagnetic field variations in Western Europe from 1500 BC to 200 AD. Part II: New intensity secular variation curve. Phys. Earth Planet. Inter. 218, 51-65.

Hervé, G., Chauvin, A., Milcent, P.-Y., Tramon, A., 2016. Archaeointensity study of five Late Bronze Age fireplaces from Corent (Auvergne, France). J. Archaeol. Sci.: Reports 7, 414-419.

Jackson, A., Jonkers, A., Walker, M., 2000. Four centuries of geomagnetic secular variation from historical records. Philos. Trans. R. Soc. Lond. Ser. A 358, 957-990.

Jonkers, A. R. T., Jackson, A., Murray, A., 2003. Four centuries of geomagnetic data from historical records. Rev. Geophys. 41, 1006.

Kovacheva, M., Boyadziev, Y., Kostadinova-Avramova, M., Jordanova, N., Donadini, F., 2009. Updated archeomagnetic data set of the past eight millennia from the Sofia laboratory, Bulgaria. Geochem. Geophys. Geosyst. 10, Q05002, doi:10.1029/2008GC002347.

Kovacheva, M., Kostadinova-Avramova, M., Jordanova, N., Lanos, P., Boyadziev, Y., 2014. Extended and revised archaeomagnetic database and secular variation curves from Bulgaria for the last eight millennia. Phys. Earth Planet. Inter. 236, 79-94, doi: 10.1016/j.pepi.2014.07.002.

Le Goff, M., Gallet, Y., 2004. A new three-axis vibrating sample magnetometer for continuous high-temperature magnetization measurements: applications to paleo- and archeo-intensity determinations. Earth Planet. Sci. Lett. 229, 31-43.

Licht, A., Hulot, G., Gallet, Y., Thébault, E., 2013. Ensembles of low degree archeomagnetic field models for the past three millennia. Phys. Earth Planet. Inter. 224, 38-67.

Lipatov, A. A., 2005. The kiln from Gorodishche (1988 excavations) in the context of lime manufacturing in Byzantine, Western Europe and Ancient Russia (in Russian). In Nosov E. N., Gorunova V.M., Plokhov A.V. Eds., Gorodishche pod Novgorodom i poselenia Severnogo Priilmeniya (Noviye materialy i issledovaniia). Saint-Petersburg, Dmitrii Bulanin, 258-393.

Lowrie, W., 1990. Identification of ferromagnetic minerals in a rock by coercivity and unblocking temperatures properties. Geophys. Res. Lett., 17, 159–162.

McIntosh, G., Kovacheva, M., Catanzariti, G., Donadini, F., Lopez, M. L. O., 2011. High coercivity remanence in baked clay materials used in archeomagnetism. Geochem. Geophys. Geosyst., 12, Q02003.

Michell, R., Forbes, N., 1914. The chronicle of Novgorod 1016-1471 (translated from the Russian). Camden Third Series Vol. XXV, London Office of the Society, pp. 237.

Nachasova, I. YE., 1972. Magnetic field in the Moscow area from 1480 to 1840 (Engl. Transl). Geomagn. Aeron. 12, 277-280.

Nasonov A. N. (Ed.), 1950. Novgorodskaya Pervaya letopis (in Russian). Izdatelstvo Akademii nauk SSSR, Moscow– Leningrad, pp. 642.

Nilsson, A., Holme, R., Korte, M., Suttie, N., Hill, M., 2014. Reconstructing Holocene geomagnetic field variation: New methods, models and implications, Geophys. J. Int. 198, 229-248.

Pavón-Carrasco, F. J., Gómez-Paccard, M., Hervé, G., Osete López, M.L., and A. Chauvin, A., 2014a. Intensity of the geomagnetic field in Europe for the last 3 ka: Influence of data quality on geomagnetic field modeling. Geochem. Geophys. Geosyst. 15, 2515-2530.

Pavón-Carrasco, F. J., Osete López, M. L., Torta, J. M., De Santis, A., 2014b. A geomagnetic field model for the Holocene based on archaeomagnetic and lava flow data. Earth Planet. Sci. Lett. 388, 98–109.

Pesonen, L. J., Leino, M. A. H., Nevanlinna, H., 1995. Archaeomagnetic intensity in Finland during the last 6400 years: Evidence for a latitude-dependent nondipole field at approximately AD 500. J. Geomagn. Geoelectr. 47, 19–40.

Rybina, E. A., 1992. Trade links of medieval Novgorod established through archaeological data. In: The archaeology of Novgorod, Russia. Recent results from the town and its hinterland. Eastern Press, Ltd, Lincoln, 193–205.

Rybina, E. A., 2001. Frühe “joint-ventures”. Die Beziehungen Novgorods im Ostseeraum. In: M. Müller-Wille u.a. (Hrsg.), Novgorod. Das mittelalterliche Zentrum und sein Umland im Norden Russlands. Studien zur Siedlungsgeschicgte und Archäologie der Ostseegebiete. 1. Neumünster, 291–308.

Spassov, S., Valet, J.-P. , Kondopoulou, D., Zananiri, I., Casas, L., Le Goff, M., 2010. Rock magnetic property and paleointensity determination on historical Santorini lava flows. Geochem. Geophys. Geosyst. 11, Q07006, doi:10.1029/2009GC003006.

Tema, E., Kondopoulou, D., 2011. Secular variation of the Earth’s magnetic field in the Balkan region during the last eight millennia based on archaeomagnetic data. Geophys. J. Int. 186(2), 603-614.

Tema, E., Gómez-Paccard , M., Kondopoulou, D., Ylenia, A., 2012. Intensity of the Earth’s magnetic field in Greece during the last five millennia: New data from Greek pottery. Phys. Earth Planet. Inter. 202–203, 14–26.

Tema, E., Morales, J., Goguitchaichvili, A., Camps, P., 2013. New archaeointensity data from Italy and geomagnetic field intensity variation in the Italian Peninsula. Geophys. J. Int. 193, 603–614.

Thellier, E., Thellier, O., 1959. Sur l'intensité du champ magnétique tesrrestre dans le passé historique et géologique. Ann. Géophys. 15, 285-376.

Yu, Y., Tauxe, L., Genevey, A., 2004. Toward an optimal geomagnetic field intensity determination technique. Geochem. Geophys. Geosyst., 5, Q02H07.

Figure captions

Fig. 1 (a) Location map of the city of Novgorod. (b) Map that identifies the location of groups of architectural brick fragments collected in the Novgorod area. 1- Church of the Annunciation in the Gorodishche (group BGA01), 2- Monastery church of St. Georgi (group GYU01), 3- Church to the Holy Apostels Peter and Paul in Silnishche (group PP01), 4- Transfiguration church on Nereditsa hill (group SN01), 5- Holy Virgin Protection church of Shilov Monastery (group SH01), 6,9- Church of the Holy Resurrection on the Derevyanitsa river (groups DM02 and DM03), 7- Church of St. Andrew the Holy Fool on Sitka (group AS01), 8- Cathedral of Our Lady of Vladimir of Syrkov Monastery (group VS01).

Fig. 2 Examples of dating via details found in the Novgorod First Chronicle (translation from Michell and Forbes, 1914) for two of our groups of brick fragments. (a) Dating of the church of the Annunciation in the Gorodishche (BGA01). (b) Dating of the church of the Holy Apostels Peter and Paul in Silnishche (PP01).

Fig. 3 Archeological context of four groups of brick fragments. (a) SN01; (b) DM02; (c) AS01; (d) SH01. See details in Fig. 1 and Table 1.

Fig. 4 Examples of low-field magnetic susceptibility versus temperature curves for our collection of fragments. The heating/cooling curves are in red/blue. The maximum temperatures were chosen relatively close to temperature T2 used for archeointensity experiments (see text). The data shown in the insets were obtained on fresh powders from the same fragments up to 700°C.

Fig. 5 IRM experiments conducted on the fragments fulfilling the criteria used to select the archeointensity results. (a) IRM curves obtained up to 0.9 T (see color code in the Figure). (b-d) Examples of hysteresis loops illustrating the three categories of IRM behavior discussed in the text. (e-g) Examples of thermal demagnetization of three-axis IRM acquired along three perpendicular directions (1.2 T, 0.4 T, 0.2 T; Lowrie, 1990).

Fig. 6 Cooling rate effect on the shape of the R(Ti) and R'(Ti) curves for fragments PP01-04 (a,b) and AS01-04 (c,d). The data were obtained using a cooling rate of 25°C/minute (a,c) vs a cooling rate of 2°C/minute (b,d). In red (resp. black) the R'(Ti) (resp. R(Ti)) data (Le Goff and Gallet, 2004). See text for further explanations.

Fig. 7 Comparison between group-mean intensity values estimated using cooling rates of 25°C/minute and 2°C/minute. The different symbols distinguish between mean intensity values determined at the fragment group level from a minimum of three different fragments (black dots) or from only two fragments (white dots; see supplementary Table S1).

Fig. 8 Archeointensity results obtained for six different groups of brick fragments. In each panel, each curve represents the R'(Ti) data obtained for one specimen (see color code on the figure). These data are first averaged at the specimen level, then a mean intensity value is estimated at the fragment level and the latter are averaged at the group level.

Fig. 9 Geomagnetic field intensity variations in the North-Western part of Russia over the past millennium. (a) Our new archeointensity data (red diamond) are compared with the data transferred to the latitude of Novgorod presently available within a radius of 700 km around Novgorod (grey dots, Nachasova, 1972; Burlatskaya et al., 1986; Pesonen et al., 1995; Kovacheva et al., 2009) and from the Balkans (light violet squares, Aitken et al., 1988, 1989; De Marco et al., 2008; Spassov et al., 2010; Kovacheva et al., 2014). The blue curve exhibits the average intensity variation curve obtained for Western Europe (Genevey et al., 2016) after its transfer to the latitude of Novgorod. (b) A comparison is also performed with the geomagnetic field intensity values expected in Novgorod from different global archeo/geomagnetic field models (see details and color code on the figure).

Table caption

Table 1 New archeointensity data obtained in Novgorod area. Location, name and dating of the different churches are indicated in columns 2 (Latitude), 3 (Longitude), 4 (Site) and 5 (Age). N/fragment (6th column) and n/specimen (7th column): number of fragments and specimens used for group-mean intensity computations. Fmean ± σF (μT) (8th column): mean intensity and its standard deviation obtained for each group of brick fragments.

Supplementary Information

Fig. S1 Archeointensity experiments performed on a pseudo-NRM acquired in known field conditions for two fragments (a) DM02-02 and (b) SH01-06 showing a large fraction of magnetization carried by hematite. The pseudo-NRM was acquired in a field of 60 μT and using a cooling rate of 25°C/minute. Triaxe experiments were conducted using the same field and cooling conditions. In red (resp. black) the R'(Ti) (resp. R(Ti)) data (Le Goff and Gallet, 2004). See text for further explanations

Fig. S2 Typical examples of thermal demagnetization of the NRM carried by specimens successfully analyzed using the Triaxe protocol (first series of measurements acquired in that protocol; see in Section 3.a and in Le Goff and Gallet, 2004). In each case, the red dot indicates the closest temperature to T1' used for archeointensity determinations.

Table S1 Archeointensity data obtained in Novgorod area both at the specimen and fragment levels. Column description: Fragment identification; Specimen identification; T1-T2, temperature interval (in °C) for intensity determination; Hlab, laboratory field used for TRM acquisition in μT; Cooling rate (°C/minute), cooling rate used for TRM acquisition; NRM T1 (T1') (%), fraction of NRM from T1' involved in intensity determination (with T1<T1'<T2); Slope R' (%), slope of the R'(Ti) data within the temperature interval of analysis; F, intensity value in μT derived for each specimen; Fmean value per fragment ± σH, mean intensity in μT computed at the fragment level with its standard deviation. *(N1/N2/N3), N1: number of fragments investigated, N2: number of fragments whose magnetization was strong enough for allowing Triaxe measurements, N3: number of fragments obeying our selection criteria.

(a)

(b)

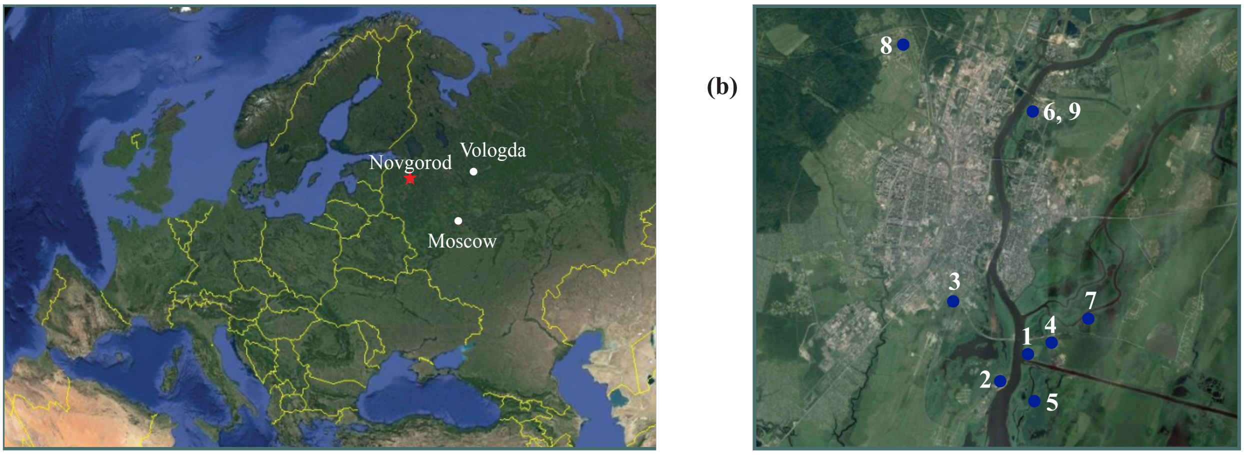

Figure 1

(a)	(b)
A.D. 1103. A.M.6611 All the brethren Knyazes of the Russian Land went against the Polovets people to the Suten, and deleated them, and captured the belongings of their Knyaz. The same year the Mordva[6] people defeated Yaroslav at Murom. The same year Knyaz Mstislav founded the Church of the Annunciation in the Gorodishche[6].	A.D. 1185. A.M. 6693. On the 1st day of May, at the 10th hour of the day, at evening bell, the sun grew dark, for an hour or more, and there were the stars; then it stone out again, and we were glad. On the 6th of the same month the people of Luki founded a stone church to the holy Apostels Peter and Paul in Silnishche. The same year Miloneg founded the stone church of the Holy Ascension under Vladyka Ilya and Knyaz Mstislav Davidovits. And in the winter David went Polotsk with the men of Novgorod and of Smolensk, and having made peace returned through Ymenets.

Figure 2

(a)

(b)

(c)

(d)

Figure 3

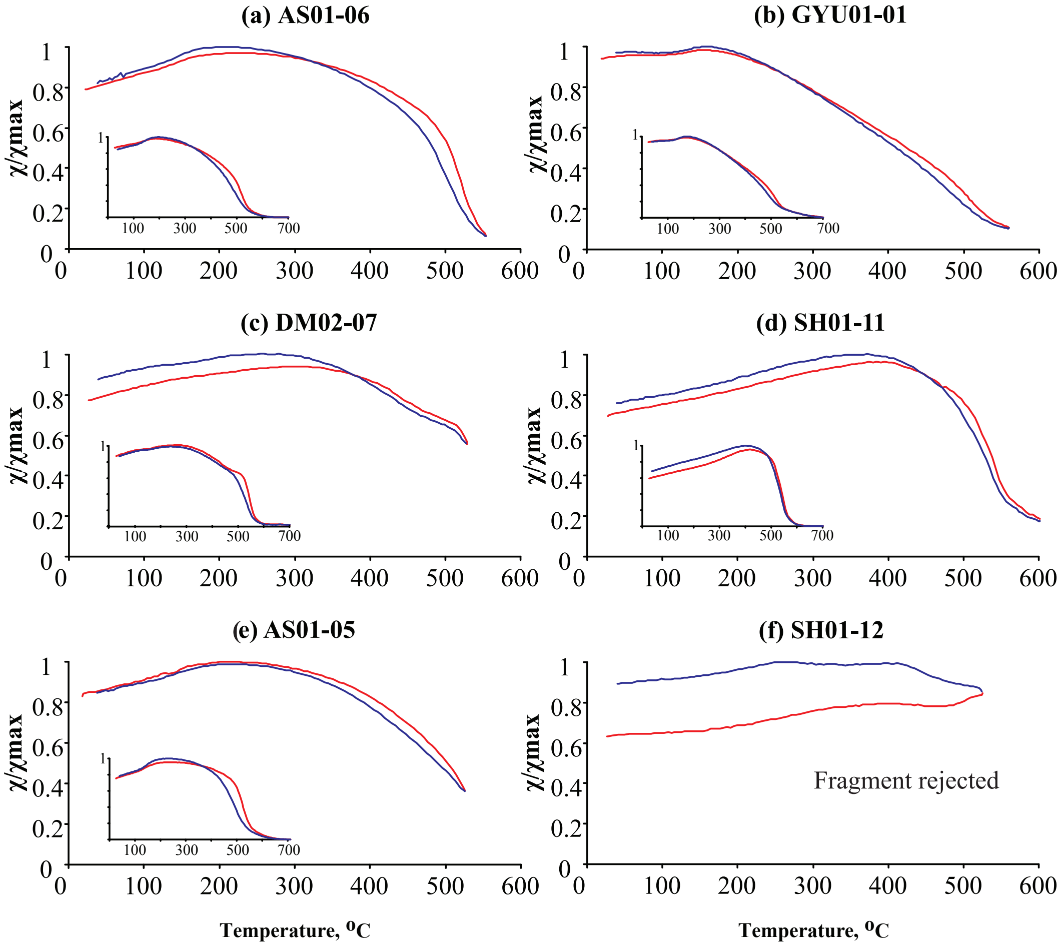
(a) AS01-06
(b) GYU01-01
(c) DM02-07
(d) SH01-11
(e) AS01-05
(f) SH01-12
χ/χmax
Temperature, ^{o}C
Fragment rejected

Figure 4

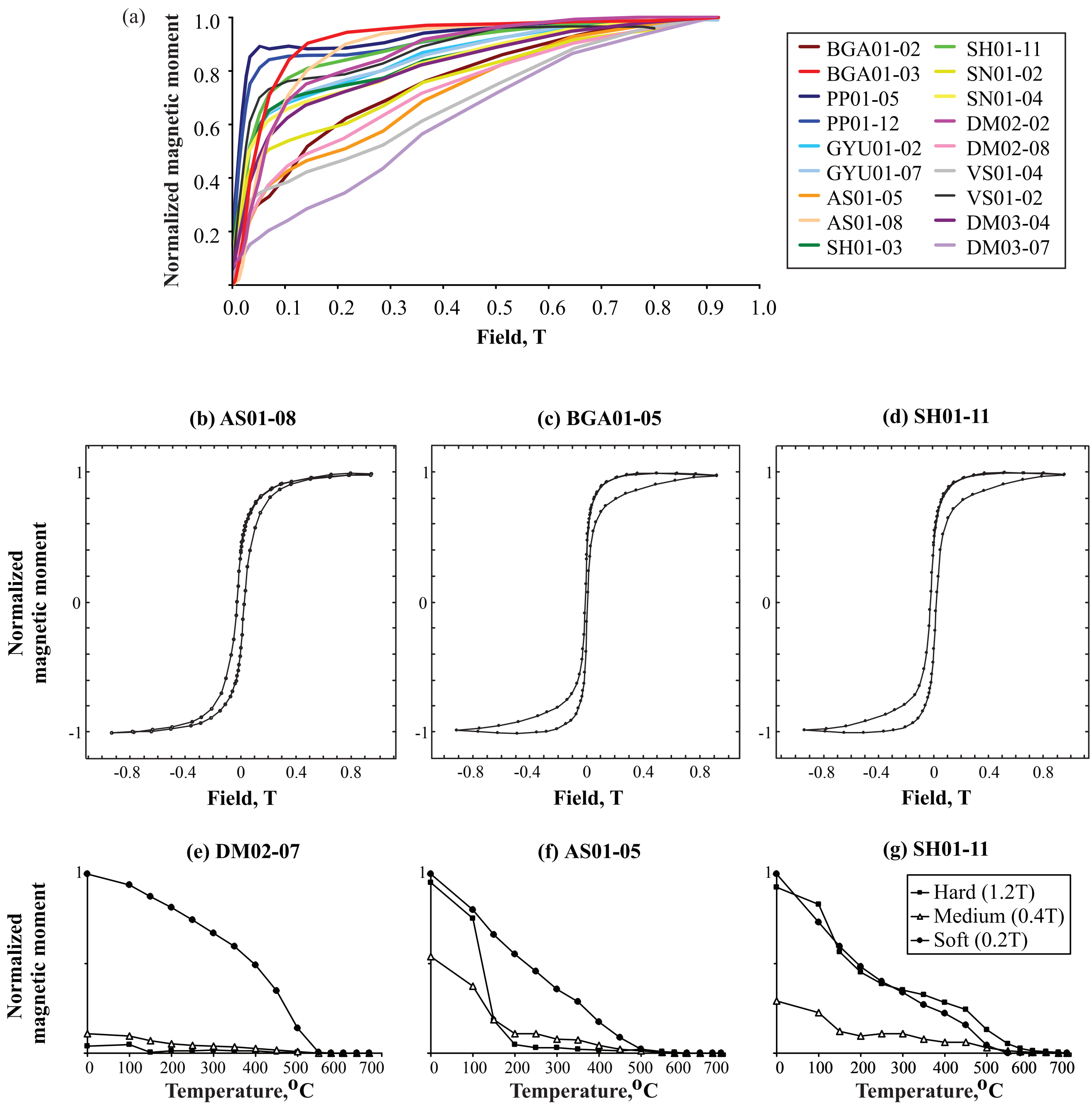
(a)
Normalized magnetic moment
1.0
0.8
0.6
0.4
0.2
0.0
0.1
0.2
0.3
0.4
0.5
0.6
0.7
0.8
0.9
1.0
Field, T
BGA01-02
BGA01-03
PP01-05
PP01-12
GYU01-02
GYU01-07
AS01-05
AS01-08
SH01-03
SH01-11
SN01-02
SN01-04
DM02-02
DM02-08
VS01-04
VS01-02
DM03-04
DM03-07
(b) AS01-08
(c) BGA01-05
(d) SH01-11
Normalized magnetic moment
1
0
-1
-0.8
-0.4
0
0.4
0.8
Field, T
(e) DM02-07
(f) AS01-05
(g) SH01-11
Normalized magnetic moment
Hard (1.2T)
Medium (0.4T)
Soft (0.2T)
0
100
200
300
400
500
600
700
Temperature,^{0}C

Figure 5

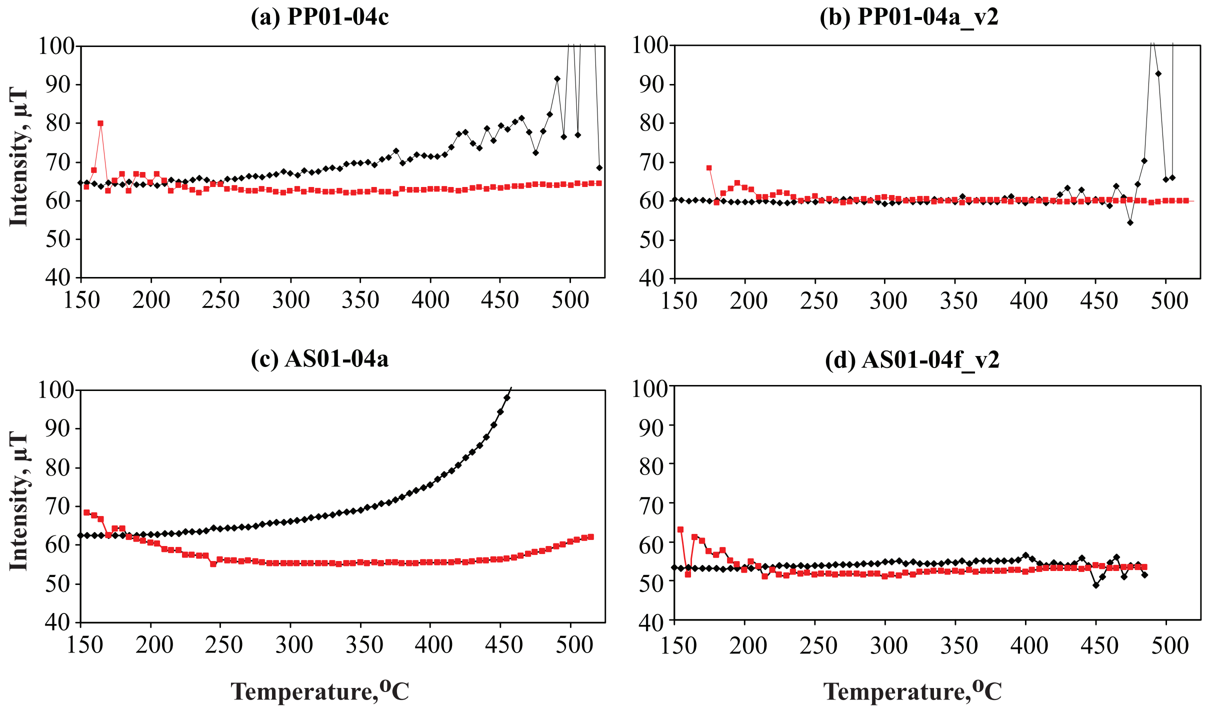

(a) PP01-04c
(b) PP01-04a_v2
(c) AS01-04a
(d) AS01-04f_v2
Intensity, µT
Intensity, µT
Temperature,⁰C
Temperature,⁰C
100
90
80
70
60
50
40
150
200
250
300
350
400
450
500

Figure 6

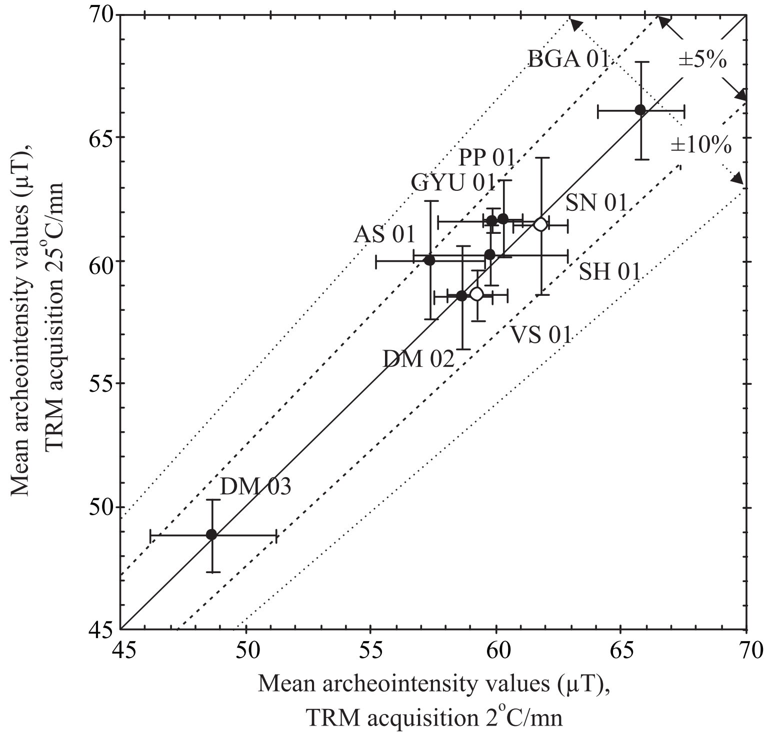

70
65
60
55
50
45
45
50
55
60
65
70
Mean archeointensity values (μT),
TRM acquisition 25°C/mn
Mean archeointensity values (μT),
TRM acquisition 2°C/mn
BGA 01
±5%
±10%
PP 01
GYU 01
SN 01
AS 01
SH 01
VS 01
DM 02
DM 03

Figure 7

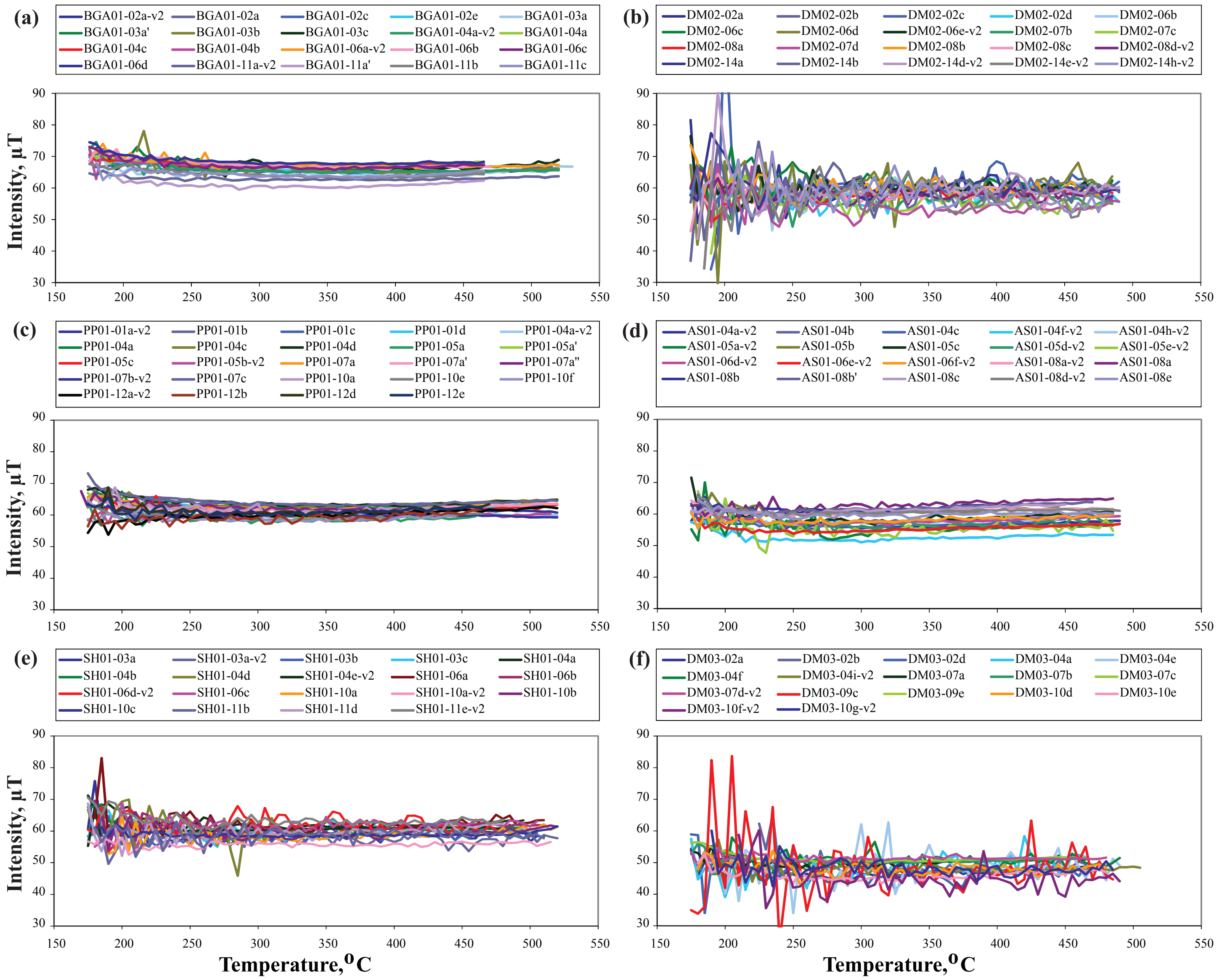
(a)
BGA01-02a-v2
BGA01-02a
BGA01-02c
BGA01-02e
BGA01-03a
BGA01-03a'
BGA01-03b
BGA01-03c
BGA01-04a-v2
BGA01-04a
BGA01-04c
BGA01-04b
BGA01-06a-v2
BGA01-06b
BGA01-06c
BGA01-06d
BGA01-11a-v2
BGA01-11a'
BGA01-11b
BGA01-11c
(b)
DM02-02a
DM02-02b
DM02-02c
DM02-02d
DM02-06b
DM02-06c
DM02-06d
DM02-06e-v2
DM02-07b
DM02-07c
DM02-08a
DM02-07d
DM02-08b
DM02-08c
DM02-08d-v2
DM02-14a
DM02-14b
DM02-14d-v2
DM02-14e-v2
DM02-14h-v2
(c)
PP01-01a-v2
PP01-01b
PP01-01c
PP01-01d
PP01-04a-v2
PP01-04a
PP01-04c
PP01-04d
PP01-05a
PP01-05a'
PP01-05c
PP01-05b-v2
PP01-07a
PP01-07a'
PP01-07a"
PP01-07b-v2
PP01-07c
PP01-10a
PP01-10e
PP01-10f
PP01-12a-v2
PP01-12b
PP01-12d
PP01-12e
(d)
AS01-04a-v2
AS01-04b
AS01-04c
AS01-04f-v2
AS01-04h-v2
AS01-05a-v2
AS01-05b
AS01-05c
AS01-05d-v2
AS01-05e-v2
AS01-06d-v2
AS01-06e-v2
AS01-06f-v2
AS01-08a-v2
AS01-08a
AS01-08b
AS01-08b'
AS01-08c
AS01-08d-v2
AS01-08e
(e)
SH01-03a
SH01-03a-v2
SH01-03b
SH01-03c
SH01-04a
SH01-04b
SH01-04d
SH01-04e-v2
SH01-06a
SH01-06b
SH01-06d-v2
SH01-06c
SH01-10a
SH01-10a-v2
SH01-10b
SH01-10c
SH01-11b
SH01-11d
SH01-11e-v2
(f)
DM03-02a
DM03-02b
DM03-02d
DM03-04a
DM03-04e
DM03-04f
DM03-04i-v2
DM03-07a
DM03-07b
DM03-07c
DM03-07d-v2
DM03-09c
DM03-09e
DM03-10d
DM03-10e
DM03-10f-v2
DM03-10g-v2
Intensity, μT
Temperature, °C
30
40
50
60
70
80
90
150
200
250
300
350
400
450
500
550

Figure 8

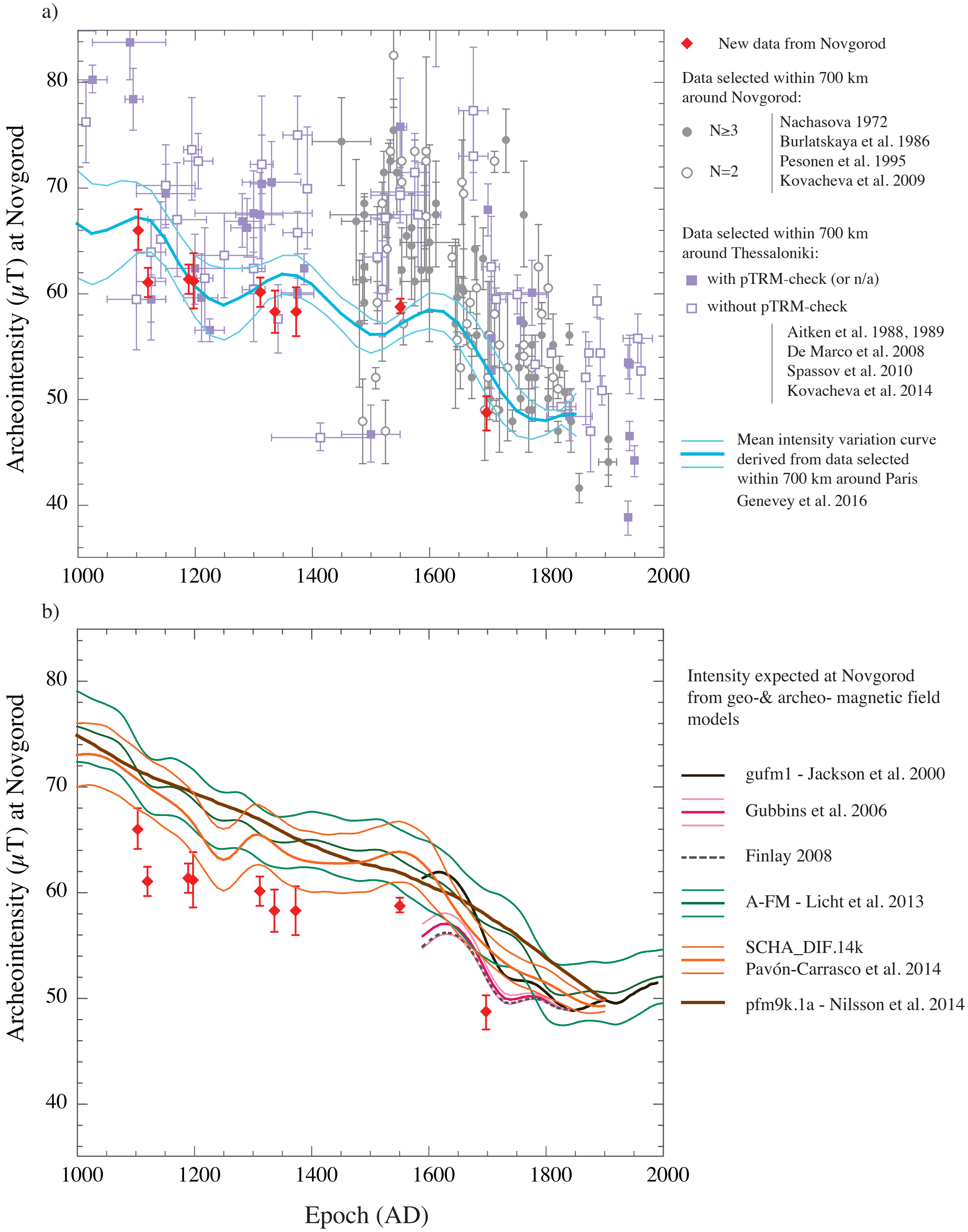

a)
b)
Archeointensity (μT) at Novgorod
Epoch (AD)
40
50
60
70
80
1000
1200
1400
1600
1800
2000
New data from Novgorod
Data selected within 700 km around Novgorod:
N≥3
N=2
Nachasova 1972
Burlatskaya et al. 1986
Pesonen et al. 1995
Kovacheva et al. 2009
Data selected within 700 km around Thessaloniki:
with pTRM-check (or n/a)
without pTRM-check
Aitken et al. 1988, 1989
De Marco et al. 2008
Spassov et al. 2010
Kovacheva et al. 2014
Mean intensity variation curve derived from data selected within 700 km around Paris
Genevey et al. 2016
Intensity expected at Novgorod from geo-& archeo- magnetic field models
gufm1 - Jackson et al. 2000
Gubbins et al. 2006
Finlay 2008
A-FM - Licht et al. 2013
SCHA_DIF.14k
Pavón-Carrasco et al. 2014
pfm9k.1a - Nilsson et al. 2014

Figure 9

Table 1

Archeomagnetic group	Lat (°N)	Long (°E)	Site	Age (AD)	N fragments	n specimens	Fmean±σF (μT)
BGA01	58.49	31.30	Church of the Annunciation in the Gorodishche	1103	5	21	66.1±1.9
GYU01	58.49	31.28	Monastery church of St. Georgi	1119	3	11	61.1±1.4
PP01	58.51	31.26	Church to the Holy Apostels Peter and Paul in Silnishche	1185 - 1192	6	25	61.4±1.4
SN01	58.50	31.31	Transfiguration church on Nereditsa hill	1198	4	17	61.2±2.6
SH01	58.48	31.30	Holy Virgin Protection church of Shilov Monastery	1310	5	20	60.1±1.4
DM02	58.56	31.30	Church of the Holy Resurrection on the Derevyanitsa river	1335	5	21	58.3±2.0
AS01	58.50	31.33	Church of St Andrew the Holy Fool on Sitka	1371	4	20	58.3±2.3
VS01	58.58	31.23	Cathedral of Our Lady of Vladimir of Syrkov Monastery	1548 - 1554	3	13	58.8±0.7
DM03	58.56	31.30	Church of the Holy Resurrection on the Derevyanitsa river	1695 – 1697	5	17	48.7±1.6

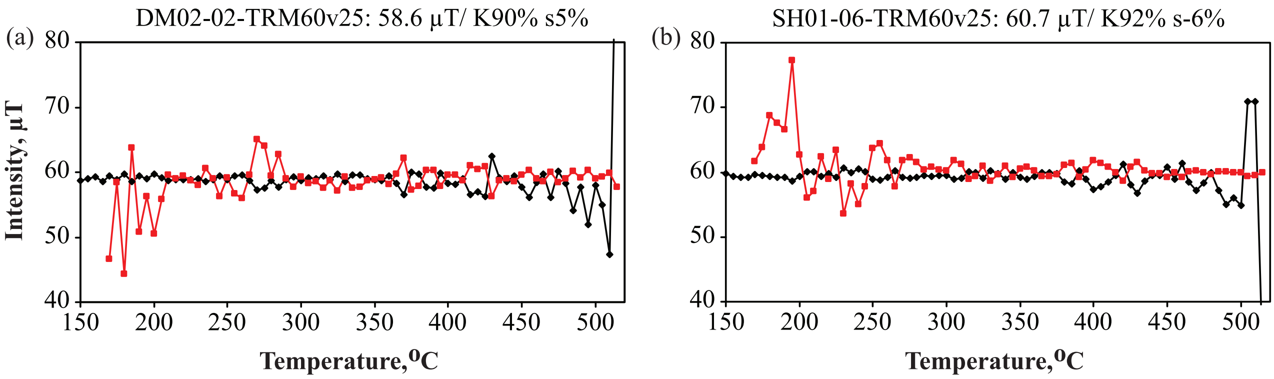

(a)
DM02-02-TRM60v25: 58.6 μT/ K90% s5%
Intensity, μT
80
70
60
50
40
150
200
250
300
350
400
450
500
Temperature,°C
(b)
SH01-06-TRM60v25: 60.7 μT/ K92% s-6%
80
70
60
50
40
150
200
250
300
350
400
450
500
Temperature,°C

Figure S1

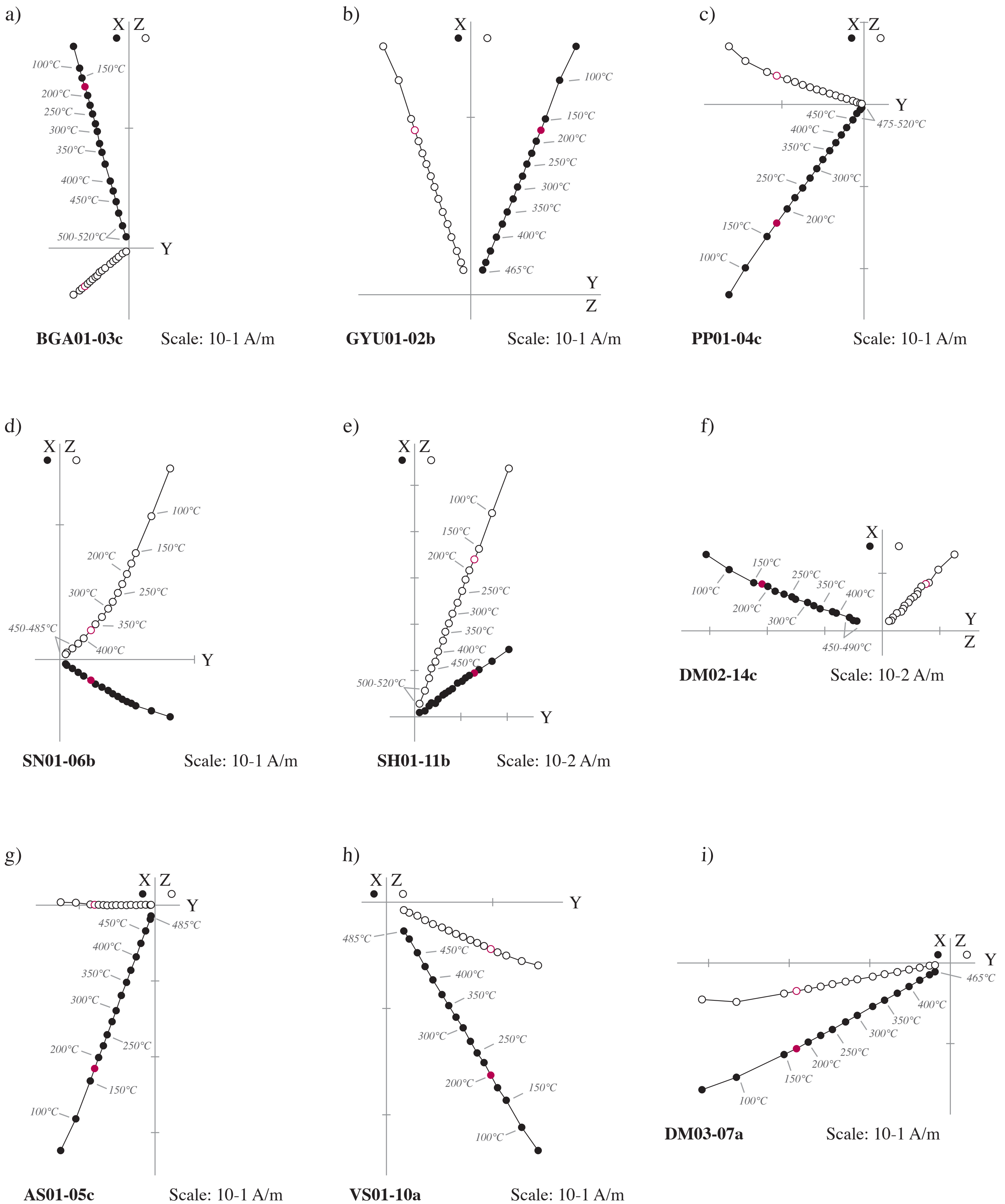
a)
X Z
Y
100°C
150°C
200°C
250°C
300°C
350°C
400°C
450°C
500-520°C
BGA01-03c
Scale: 10-1 A/m
b)
X
Y
Z
100°C
150°C
200°C
250°C
300°C
350°C
400°C
465°C
GYU01-02b
Scale: 10-1 A/m
c)
X Z
Y
450°C
400°C
350°C
475-520°C
250°C
300°C
200°C
150°C
100°C
PP01-04c
Scale: 10-1 A/m
d)
X Z
Y
100°C
150°C
200°C
250°C
300°C
350°C
400°C
450-485°C
SN01-06b
Scale: 10-1 A/m
e)
X Z
Y
100°C
150°C
200°C
250°C
300°C
350°C
400°C
450°C
500-520°C
SH01-11b
Scale: 10-2 A/m
f)
X
Y
Z
100°C
150°C
200°C
250°C
300°C
350°C
400°C
450-490°C
DM02-14c
Scale: 10-2 A/m
g)
X Z
Y
450°C
485°C
400°C
350°C
300°C
250°C
200°C
150°C
100°C
AS01-05c
Scale: 10-1 A/m
h)
X Z
Y
485°C
450°C
400°C
350°C
300°C
250°C
200°C
150°C
100°C
VS01-10a
Scale: 10-1 A/m
i)
X Z
Y
465°C
400°C
350°C
300°C
250°C
200°C
150°C
100°C
DM03-07a
Scale: 10-1 A/m

Figure S2

Fragment	Specimen	T_{min} - T_{max} (^{o} C)	F_{Lab}	Cooling rate, (^{o} C/mn)	NRM T1 (T1') (%)	Slope R' (%)	F_{Triaxe} (μT)	$F_{Triaxe\ mean}$ value per fragment ±σF (μT)
1	2	3	4	5	6	7	8	9
BGA01, Novgorod, The Church of the Annunciation in the Gorodishche, [1103] AD, (12/12/5)								
BGA01-02	BGA01-02a	175−465	65	25	83	-8	65.8	
	BGA01-02c	175−515	65	25	92	-2	65.5	66.0±0.4
	BGA01-02e	175−465	65	25	83	-6	66.1	
	BGA01-02a-v2	180−520	65	2	96	-6	66.5	
BGA01-03	BGA01-03a	180−530	65	25	95	-2	65.2	
	BGA01-03a'	205−465	65	25	65	-5	67.3	66.4±1.0
	BGA01-03c	180−520	65	25	89	-2	67.1	
	BGA01-03b-v2	210−520	65	2	95	-5	66.0	
			65					
BGA01-04	BGA01-04b	175−465	65	25	87	-2	68.0	
	BGA01-04c	175−465	65	25	86	-2	67.5	67.3±0.9
	BGA01-04d	175−465	65	25	90	-2	67.6	
	BGA01-04a-v2	175−520	65	2	95	-5	65.9	
BGA01-06	BGA01-06b	175−470	65	25	84	-6	67.6	
	BGA01-06c	175−465	65	25	84	-5	67.3	67.8±0.6
	BGA01-06d	175−465	65	25	84	-5	68.6	
	BGA01-06a-v2	180−520	65	2	96	-5	67.7	
BGA01-11	BGA01-11a	205−445	65	25	66	-4	61.8	
	BGA01-11a'	195−465	65	25	79	0	60.9	
	BGA01-11b	175−465	65	25	79	-5	64.4	62.9±1.5
	BGA01-11c	180−465	65	25	74	-1	64.3	
	BGA01-11a-v2	175−520	65	2	95	-1	63.0	
GYU01, Novgorod, The monastery Church of St. Georgi, [1119] AD, (7/7/3)								
GYU01-01	GYU01-02b	180−465	65	25	78	-3	61.6	
	GYU01-02c	215−485	65	25	55	8	60.5	59.7±1.7
	GYU01-02a-v2	175−485	65	2	89	4	58.0	
	GYU01-02e-v2	180−465	65	2	69	3	58.5	
GYU01-04	GYU01-04a-v2	180−485	65	2	91	1	62.0	
	GYU01-04d-v2	180−485	65	2	91	-1	62.4	62.4±0.4
	GYU01-04f-v2	175−480	60	2	91	-2	62.7	
GYU01-07	GYU01-07a	215−485	65	25	56	5	61.5	
	GYU01-07b	200−485	65	25	51	2	61.5	61.4±1.7
	GYU01-07c	175−485	65	25	67	-4	63.3	
	GYU01-07f-v2	175−480	60	2	87	0	59.1	

1	2	3	4	5	6	7	8	9
PP01, Novgorod, The Church to the Holy Apostels Peter and Paul in Silnishche, [1185 – 1192] AD, (12/10/6)								
PP01-01	PP01-01b	175−510	60	25	95	-5	64.3	62.7±1.1
	PP01-01c	180−510	60	25	96	-3	62.1	
	PP01-01d	180−510	60	25	96	-1	62.6	
	PP01-01a-v2	200−520	60	2	97	-4	61.9	
PP01-04	PP01-04a	175−440	60	25	80	-4	63.0	62.8±1.6
	PP01-04c	175−520	60	25	96	-1	63.7	
	PP01-04d	175−520	60	25	96	-3	64.0	
	PP01-04a-v2	195−520	60	2	98	-3	60.4	
PP01-05	PP01-05c	185−520	60	25	92	0	61.4	60.0±1.1
	PP01-05a	175−460	60	25	76	-2	58.8	
	PP01-05a'	175−445	60	25	70	-5	60.1	
	PP01-05b-v2	175−515	60	2	93	1	59.7	
PP01-07	PP01-07a	175−520	60	25	97	-2	62.7	62.3±1.5
	PP01-07a'	180−520	60	25	97	1	62.2	
	PP01-07a''	170−465	60	25	88	-6	62.6	
	PP01-07c	175−520	60	25	97	-5	64.2	
	PP01-07b-v2	175−520	60	2	97	-3	60.0	
PP01-10	PP01-10a	175−460	60	25	85	-4	61.8	59.9±1.3
	PP01-10e	175−465	60	25	84	-2	59.4	
	PP01-10f	175−445	60	25	81	0	58.7	
	PP01-10a-v2	170−505	60	2	91	-1	59.6	
PP01-12	PP01-12b	175−465	60	25	78	5	59.1	60.4±1.1
	PP01-12d	185−465	60	25	75	0	61.4	
	PP01-12e	175−465	60	25	76	1	61.2	
	PP01-12a-v2	175−520	60	2	93	9	60.0	
SN01, Novgorod, The Transfiguration church on Nereditsa hill, [1198] AD, (11/9/4)								
SN01-02	SN01-02a	190−485	60	25	91	1	61.0	60.8±0.8
	SN01-02a'	200−465	60	25	79	-4	59.6	
	SN01-02b	205−465	60	25	81	2	61.2	
	SN01-02c	200−465	60	25	82	-3	61.6	
	SN01-02d-v2	195−480	60	2	91	-3	60.7	
SN01-04	SN01-04a	175−485	60	25	91	-3	57.5	57.9±2.6
	SN01-04b	180−485	60	25	74	0	55.6	
	SN01-04c	175−480	60	25	90	-7	60.7	
SN01-06	SN01-06b	375−485	60	25	79	3	62.6	64.2±1.8
	SN01-06d	350−485	60	25	78	3	65.9	
	SN01-06e	375−485	60	25	75	2	65.6	
	SN01-06f-v2	375−485	60	2	73	5	62.8	

1	2	3	4	5	6	7	8	9
SN01-09	SN01-09a	395−485	60	25	86	-1	62.4	
	SN01-09b	395−485	60	25	87	3	61.6	
	SN01-09c	395−485	60	25	87	4	63.4	62.0±1.1
	SN01-09d	385−485	60	25	88	6	62.2	
	SN01-09e	380−485	60	25	89	4	60.3	
SH01, Novgorod, Holy Virgin Protection church of Shilov monastery, [1310] AD, (8/8/5)								
SH01-03	SH01-03a	175−510	60	25	75	-1	59.1	
	SH01-03b	175−505	60	25	73	2	59.1	59.2±1.1
	SH01-03c	175−505	60	25	74	-1	60.6	
	SH01-03a-v2	180−510	60	2	74	-3	57.8	
SH01-04	SH01-04a	175−495	60	25	95	-6	62.6	
	SH01-04b	175−495	60	25	93	-5	60.2	61.1±1.1
	SH01-04d	175−480	60	25	81	-1	61.2	
	SH01-04e-v2	175−480	60	2	86	3	60.5	
SH01-06	SH01-06a	180−510	60	25	77	-1	62.4	
	SH01-06b	205−510	60	25	74	0	61.3	61.8±0.5
	SH01-06c	180−505	60	25	75	5	61.5	
	SH01-06d-v2	175−475	60	2	55	-1	61.8	
SH01-10	SH01-10a	190−520	60	25	86	5	58.7	
	SH01-10b	180−520	60	25	94	-2	59.6	58.2±1.7
	SH01-10c	180−520	60	25	86	0	58.9	
	SH01-10a-v2	175−515	60	2	92	1	55.7	
SH01-11	SH01-11b	180−520	60	25	86	1	58.8	
	SH01-11c	180−520	60	25	85	-6	59.3	60.3±2.1
	SH01-11d	175−480	60	25	53	4	59.6	
	SH01-11e-v2	175−480	60	2	53	-4	63.4	
DM02, Novgorod, Church of the Holy Resurrection by the river Derevyanitsa, [1335]AD, (10/9/5)								
DM02-02	DM02-02a	175−485	65	25	61	5	58.9	
	DM02-02b	175−485	65	25	70	6	58.1	58.9±1.2
	DM02-02c	190−490	65	25	64	2	60.5	
	DM02-02d	175−490	65	25	69	-1	57.9	
DM02-06	DM02-06b	225−490	65	25	73	6	59.5	
	DM02-06c	175−485	65	25	72	-6	61.7	60.4±0.9
	DM02-06d	175−485	65	25	69	8	60.2	
	DM02-06e-v2	175−480	60	2	64	-3	60.1	
DM02-07	DM02-07b	195−485	65	25	64	-1	56.2	
	DM02-07c	190−485	65	25	63	-2	55.0	55.0±1.3
	DM02-07d	190−490	65	25	62	-3	53.7	
DM02-08	DM02-08a	175−485	65	25	66	6	57.7	
	DM02-08b	175−485	65	25	66	-7	60.1	58.4±1.1
	DM02-08c	175−485	65	25	64	5	57.9	
	DM02-08d-v2	175−485	60	2	65	-5	58.0	

1	2	3	4	5	6	7	8	9
DM02-14	DM02-14a	175−490	65	25	59	-5	60.2	58.9±1.7
	DM02-14b	175−490	65	25	70	0	59.6	
	DM02-14c	185−490	65	25	69	-2	59.7	
	DM02-14d	180−490	65	2	57	-6	60.3	
	DM02-14e	185−485	60	2	66	1	56.4	
	DM02-14h	200−480	60	2	64	-7	57.2	
AS01, Novgorod, The church of St Andrew the Holy Fool on Sitka, [1371] AD, (11/6/4)								
AS01-04	AS01-04b	175−470	65	25	78	1	58.1	56.4±2.2
	AS01-04c	175−450	65	25	60	-1	56.9	
	AS01-04a-v2	175−490	65	2	82	0	56.7	
	AS01-04f-v2	175−485	60	2	91	-1	52.7	
	AS01-04h-v2	175−445	60	2	68	-2	57.8	
AS01-05	AS01-05b	180−445	65	25	74	-2	61.1	57.7±2.4
	AS01-05c	175−485	65	25	90	-1	59.2	
	AS01-05a-v2	175−485	65	2	89	-2	55.7	
	AS01-05d-v2	180−485	60	2	82	-2	57.0	
	AS01-05e-v2	180−485	60	2	76	-2	55.7	
AS01-06	AS01-06d-v2	180−490	60	2	86	2	58.0	57.2±1.6
	AS01-06e-v2	180−490	60	2	90	3	55.4	
	AS01-06f-v2	175−485	60	2	89	3	58.2	
AS01-08	AS01-08a	175−485	65	25	72	7	62.9	61.6±1.1
	AS01-08b	180−450	65	25	84	3	61.9	
	AS01-08b'	180−470	65	25	81	4	62.0	
	AS01-08b''	175−485	65	25	88	4	63.3	
	AS01-08c	175−450	65	25	80	5	61.3	
	AS01-08d-v2	180−490	60	2	90	1	60.8	
	AS01-08e-v2	180−485	60	2	88	-1	60.0	
	AS01-08a-v2	175−485	65	2	84	2	60.9	
VS01, Novgorod, Cathedral of Our Lady of Vladimir in Syrkov Monastery, [1548 − 1554] AD, (11/5/3)								
VS01-02	VS01-02a	200−465	50	25	58	-9	58.5	58.5±2.2
	VS01-02b	180−465	50	25	66	6	55.4	
	VS01-02d	195−465	60	25	58	-8	59.5	
	VS01-02a-v2	175−510	50	2	90	-8	60.5	
VS01-04	VS01-04b	175−485	50	25	82	0	61.0	58.3±1.6
	VS01-04c	175−465	60	25	66	3	57.0	
	VS01-04d	175−485	60	25	62	-5	58.5	
	VS01-04f	175−465	60	25	68	1	57.0	
	VS01-04a-v2	175−510	50	2	86	-6	58.1	
VS01-10	VS01-10a	195−485	50	25	77	-3	59.5	59.7±0.2
	VS01-10b	200−465	60	25	63	-5	59.6	
	VS01-10c	180−465	60	25	70	-8	60.0	
	VS01-10d	200−465	60	25	61	-2	59.6	

1	2	3	4	5	6	7	8	9
DM03, Novgorod, Church of the Holy Resurrection by the river Derevyanitsa, [1695 – 1697] AD, (11/8/5)								
DM03-02	DM03-02a	175−465	50	25	70	-2	47.2	47.6±1.3
	DM03-02b	225−465	50	25	62	-9	49.1	
	DM03-02d	175−470	50	25	61	-4	46.5	
DM03-04	DM03-04a	175−465	50	25	60	10	48.6	49.1±1.0
	DM03-04e	195−490	50	25	57	2	49.1	
	DM03-04f	190−490	50	25	55	-1	50.5	
	DM03-04i-v2	180−505	50	2	51	-4	48.2	
DM03-07	DM03-07a	175−465	50	25	86	1	50.2	50.9±0.6
	DM03-07b	175−465	50	25	84	-1	50.6	
	DM03-07c	175−465	50	25	84	-4	51.4	
	DM03-07d	175−480	50	2	90	-1	51.4	
DM03-09	DM03-09c	175−485	50	25	53	-3	48.2	49.2±1.0
	DM03-09e	175−480	50	25	56	-3	50.1	
DM03-10	DM03-10d	180−480	50	25	53	-2	47.9	46.7±1.6
	DM03-10e	180−480	50	25	56	0	46.1	
	DM03-10f-v2	210−490	50	2	54	-9	44.7	
	DM03-10g-v2	190−485	50	2	60	-7	48.2	